Bilayered Potassium Vanadate K0.5V2O5 as Superior Cathode Material for Na-ion Batteries

Rita Baddour-Hadjean, Le Than Nguyen Huyhn, Daureen Batyrbekuly, Stephane Bach, Jean Pierre Pereira-Ramos

Bilayered Potassium Vanadate $K_{0.5}V_2O_5$ as Superior Cathode Material for Na-ion Batteries

R. Baddour-Hadjean[1*], L. T. N. Huyhn[1], D. Batyrbekuly[1,2], S. Bach[1,3], J. P. Pereira-Ramos[1*]

[1]*Institut de Chimie et des Matériaux Paris Est (ICMPE), GESMAT, UMR 7182 CNRS-Université Paris Est Créteil, 2 rue Henri Dunant, 94320 Thiais, France*

[2] *School of Engineering, National Laboratory Astana, Nazarbayev University, 53 Kabanbay Batyr Avenue, Astana 010000, Kazakhstan*

[3]*Université d'Evry Val d'Essonne, Dept Chimie, Bd F. Mitterrand, 91000 Evry, France*

Corresponding authors: baddour@icmpe.cnrs.fr Tel. 33 1 49 78 11 55

pereira@icmpe.cnrs.fr Tel. 33 1 49 78 12 79

Abstract: A bilayered potassium vanadate $K_{0.5}V_2O_5$ (KVO) is synthesized by a fast and facile synthesis route and evaluated as positive electrode material for Na-ion batteries. Half the potassium ions can be topotactically extracted from KVO through the first charge, allowing then 1.14 Na^+ ions to be reversibly inserted. A good rate capability is also highlighted, with 160 mAh g^{-1} at C/10, 94 mAh g^{-1} at C/2, 73 mAh g^{-1} at 2C and excellent cycling stability with 152 mAh g^{-1} still available after 50 cycles at C/10. *Ex-situ* X-ray diffraction reveals weak and reversible structural changes consisting in soft breathing of KVO host lattice upon Na extraction-insertion cycles ($\Delta V/V \approx 3\%$). A high steadiness of the structure is also evidenced upon cycling, at both the long-range order and atomic scale probed by Raman spectroscopy. This remarkable behavior is ascribed to the large interlayer space of KVO (≈ 9.5 Å) stabilized by pillar K ions, able to accommodating Na ions without critical change in the structure. Kinetics measurements reveal a good Na diffusivity that is little affected upon discharge. This study opens further exploration of potassium vanadates and other bronzes in the field of Na-ion batteries.

1. Introduction

With the rapid development of renewable energy sources, the deployment of new Electrical Energy Storage solutions is highly desired. Lithium-ion batteries (LIBs), which dominate the portable electronic market, are expected to answer this requirement [1]. However, the use of Li is impeded by its high cost, limited reserves and uneven distribution [2]. As a result, research has turned to batteries composed of low-cost and earth-abundant elements, among them Na-ion batteries have been highlighted as one of the best alternatives to LIBs because their reaction mechanism is similar to that of LIBs and Na sources are essentially unlimited [3-13].

To date, a large variety of Na-insertion frameworks have been proposed as cathode materials [14-19]. Similar to LIBs, highly reversible cathode materials based upon the intercalation reaction are needed for high capacity and good cyclability of SIBs. These cathode materials are mainly categorized into oxides and polyanion types [14]. A major obstacle is the difficulty to get a sodium host material with comparable operating voltage and capacity to LIBs analogs. Among the transition metal oxides investigated as cathode materials the group of vanadium oxides and bronzes has been screened, most of them in the last years: V_2O_5 polymorphs [20-22], bilayered V_2O_5 [23, 24], $Na_{0.33}V_2O_5$ [25-27], Na_xVO_2 [28, 29], $NaVO_3$ [30], NaV_3O_8 [31], γ-NaV_2O_5 [32]. More recently, we reported a novel Li intercalation compound, the potassium vanadium bronze $K_{0.5}V_2O_5$ synthesized via a fast and facile solution route [33]. This cathode material was found to exhibit outstanding electrochemical performance, one of the best among the vanadium bronzes, with a specific capacity of 210 mAh g^{-1} at an average voltage of 2.9 V vs. Li^+/Li, without any significant structural changes after extended cycling experiments. An excellent capacity retention was also reported, with still 200 mAh g^{-1} at C/10 after 70 cycles and a good rate capability with 140 mAh g^{-1} at 1C. This attractive behaviour originates from the unusually large *d*-spacing of 7.7

Å practically twice that of the parent oxide V_2O_5, and the presence of interlayer K^+ ions that stabilize the stacking of double-sheet V_2O_5 layers.

Motivated by the great electrochemical performance of vanadium oxides and bronzes in LIBs and NIBs, we investigate in the present work $K_{0.5}V_2O_5$ (named KVO) as a potential candidate for cathode material of SIBs. Electrochemical study show that this material is capable to deliver a reversible Na-ion storage capacity around 160 mAh g^{-1} at the current density of C/10 in the voltage range of 1.5 - 4 V vs. Na^+/Na. It also demonstrates a good rate capability with a capacity of 94 mAh g^{-1} at C/2 and still 73 mAh g^{-1} at 2C and excellent cycling stability with 158 mAh g^{-1} still available after 50 cycles at C/10. Ex-situ X-ray diffraction and Raman spectroscopy reveal the high structural steadiness of this layered potassium vanadate. A kinetic study of Na transport shows a limited impact of depth of discharge on sodium diffusion rate. Given the facile synthesis and great diversity of potassium vanadates, this study may stimulate further exploration of guest species insertion/deinsertion in this appealing family of compounds.

2. Results and discussion

SEM images (**Fig. 1**) show the KVO powder exhibits well-defined and regular platelets of about 10 µm long, 1 µm wide and 0.5 µm thick, with homogeneous distribution throughout the sample. The XRD pattern of the KVO powder (**Fig. 2**) can be indexed into monoclinic δ-$K_{0.486}V_2O_5$ structure *C2/m* (Z = 4) [JCPDS 0860347] isomorphic to that of $Na_{0.56}V_2O_5$ and δ-$Ag_{0.68}V_2O_5$, with lattice parameters a = 11.659 Å, b = 3.668 Å; c = 9.469 Å, $\alpha = \gamma = 90°$, $\beta = 92.24°$. Small impurity of monoclinic $K_{0.25}V_2O_5$ is found (*200* reflection at ca. 14°). This result is consistent with previous studies performed on single crystals and powders [33-36]. In our experiments, *00l* lines exhibit high relative intensities, which suggest a high-preferred orientation, as previously observed on

microwave-synthesized powders [35]. However, in the latter case larger particles with many defects and a heterogeneous size distribution were obtained. Inset in **Fig. 2** illustrates the crystal structure of KVO : two single sheets made of octahedral VO_6 are linked together alternately by edge sharing to from the double-sheet V_2O_5 layered structure, the K-ions lying between the layers, yielding a sandwiched structure.

$K_{0.5}V_2O_5$ belongs to the *C2h* point symmetry group. Factor group analysis yields the allowed representations for each one of the selected Wyckoff (**Table 1**).

Atoms in $K_{0.5}V_2O_5$ unit cell	Wyckoff position	Γ(i)
V[1],V[2],K,O[1],O[2],O[3],O[4],O[5]	4i	$2A_g + B_g + A_u + 2B_u$

Table 1. Allowed representation for each atom in $K_{0.5}V_2O_5$ crystal

Summarizing the overall contribution and subtracting the acoustic modes ($\Gamma_{ac}= A_u+2B_u$), we obtain the following irreducible representations of $K_{0.5}V_2O_5$ vibrational modes:

$$\Gamma(\ K_{0.5}V_2O_5) = 16A_g + 8B_g + 7A_u + 14B_{2u}$$

Thus, 24 Raman active modes are expected to show up in the Raman spectrum of KVO. In this study, as in many spectroscopic studies of solids, the number of modes experimentally observed is significantly lower than that predicted by group theory methods. This situation occurs because of small polarizability derivatives for many Raman active modes and small frequency shift separation components, e.g. B_g modes almost coincide with A_g modes. The Raman spectrum of the as-obtained powder (**Fig. 2b**) shows the typical fingerprint previously reported for KVO, consisting of 20 bands located at 86, 98, 136, 169, 231, 260, 274, 330, 345, 410, 504, 600, 697, 783, 842, 883, 944, 960, 978 and 1007 cm^{-1}.

A detailed assignment of this Raman spectrum can be found in [34]. Briefly, most of the observed modes correspond to the stretching and bending vibrations of the different V-O and V-O-V bonds. In the 200-900 cm^{-1} frequency region, the observed bands have their counterpart in the Raman spectrum of V_2O_5 crystal and are assigned to the δ(V-O-V) bending and ν(V-O) stretching vibrations in the $(V)O_6$ octahedra [37, 38]. In the 900-1020 cm^{-1} range, the stretching vibrations of the two shortest apical V=O bonds (d ≈ 1.6 Å) are observed (**see inset in Fig. 2b**). Multiple features (at 944, 960, 978 and 1007 cm^{-1}) are clearly highlighted in this region for KVO compared to two bands at 995 cm^{-1} and 976 cm^{-1} in V_2O_5. This multiplicity is due to the presence of two short bonds in KVO instead of a single one in V_2O_5, combined with the existence of both V^{4+}=O and V^{5+}=O species in the potassium bronze. Worth is also noting intense Raman features at 783 and 883 cm^{-1} that correspond to the stretching vibrations of strongly asymmetric V_1-O_1-V_2 and V_1-O_3-V_2 bridges in the double layer structure of KVO (**see inset in Fig. 2b**)**.** Finally, Raman features below 200 cm^{-1} are associated to the modes involving displacements of vanadium atoms.

The electrochemical properties of KVO were examined in sodium half-cell. **Fig. 3a** presents the first discharge-charge cycle of KVO at C/10 rate. Starting from the open circuit voltage of 3.29 V vs. Na^+/Na, 0.36 Na^+ ions can be intercalated in KVO at an average potential of 2.45 V, corresponding to a specific capacity of 49 mAh g^{-1}. Then, the oxidation reaction proceeds along two plateaus at 2.71 V and 3.57 V and involves a total capacity of 0.62 F/mol. This result indicates that not only 0.36 sodium ions can be reversibly extracted along the first plateau but also additional potassium extraction takes place along the second plateau at 3.57 V (c.a. 0.26 K^+/mol). The participation of SEI can be excluded because it occurs at higher voltage of 4.5 V. Hence, after the first cycle, the composition of the oxidized electrode is ≈ $K_{0.24}V_2O_5$. The following discharge-charge cycles are shown in **Fig. 3b**. The faradaic yield progressively increases with cycles, from

0.96 Na^+/mole (134 mAh g^{-1}) for cycle 2 to 1.14 Na^+/mole (160 mAh g^{-1}) for cycle 10. A quantitative charge process is obtained, showing the excellent reversibility of the Na insertion-extraction process. Further cycling show the discharge-charge curves superimpose with an excellent capacity retention since 152 mAh g^{-1} and 140 mAh g^{-1} are still available after 50 and 80 cycles at C/10, respectively (**Fig. 3c**) and still 130 mAh g^{-1} after 100 cycles at various C-rate between C/10 and 5C (**Fig. 3d**). **Fig 3d** shows the results of rate capability tests from C/10 to 5C.

Whatever the C rate, a good stability is obtained. The capacity decreases from 144 mAh g^{-1} at C/10 to 106 mAh g^{-1} at C/5, 94 mAh g^{-1} at C/2 and still 73 mAh g^{-1} at 2C. A significant drop in capacity is seen only for 5C (≈ 40 mAh g^{-1}) but the same value of 94 mAh g^{-1} recovered at C/2 indicates that the structure can support high C-rate without irreversible damages. Except the bilayered V_2O_5 nanobelts [24] and the ε'-V_2O_5 phase [22] delivering near 200 mAh g^{-1}, the present KVO exhibits the highest capacity with a maximum value of 160 mAh g^{-1}. Indeed, most of capacity values obtained for V_2O_5 oxides, bronzes and derivates do not exceed 120-150 mAh g^{-1} [20-21, 25-32].

We have investigated the structural changes during the Na-insertion-extraction process in KVO. The XRD patterns and Raman spectra series of KVO electrodes are shown in **Figs. 4 and 5**, respectively. For this highly oriented material, the evolution of the *001* reflection line (**Fig. 4a**) is of particular interest. We have checked that the first reduction process involving the insertion of ≈ 0.36 Na ions in KVO (**Fig. 3a**) keeps the structure of the pristine KVO material. Only a decrease in the *c* parameter value is found, from 9.49 Å in the pristine material to 9.07 Å for the reduced $Na_{0.36}$KVO electrode. A reverse trend is evidenced upon the oxidation involving sodium and potassium extraction. Indeed, the departure of large interlayer cations results in stronger repulsions

between the negative V_2O_5 layers and consequently the corresponding interlayer *c* parameter increases from 9.07 to 9.32 Å. Then, during the second discharge, further Na insertion in KVO induces a slight interlayer decrease, as shown by the progressive shift toward higher angle observed in the $0.2 \leq x \leq 1$ composition range (**Fig. 4a)**, to reach *c* = 9.02 Å for the fully reduced Na_1KVO composition ($\Delta c/c \approx 3\%$). Once again, a reverse trend is observed upon Na extraction, with a *c* value of 9.30 Å recovered after the second cycle. Remarkably, the XRD pattern of an electrode after 50 cycles (**Fig. 4b**) is superimposable to the one after one cycle, showing the high stability of the structure upon cycling and no amorphization phenomenon. It can be indexed in the same monoclinic *C2/m* symmetry, with unit cell parameters of *a* = 11.54 Å, *b* = 3.47 Å; *c* = 9.30 Å. The Raman spectra evolution during the second discharge (**Fig. 5**) show a progressive band broadening probably due to an increase in the electronic conductivity of the material on sodiation. However, a remarkable recovering of the KVO Raman fingerprint is observed after cycles, indicating the in-plane structural arrangement of KVO layers is not affected, even upon extended cycling. Furthermore, the Raman spectrum obtained after 50 cycles does not make evidence of any new band due to the presence of parasite phase formed at the electrode surface during cycling.

These results demonstrate the high stability of the bilayered structure of KVO. The existence of a large interlayer space combined to the presence of K^+ ions, acting as pillar species, makes possible the reversible insertion of up to 1.14 sodium ions. As observed in the case of lithium insertion [33], the layered structure of KVO, characterized by a large interlayer spacing of 9.5 Å, twice that encountered in the V_2O_5 parent oxide ($\approx$ 4.37Å), probably explains a facile and reversible Na insertion-extraction process.

The electrochemical kinetics of Na insertion into KVO has been investigated using impedance spectroscopy. The Nyquist diagrams obtained during the discharge are shown in **Fig. 6a**. All the

diagrams show a well-defined high frequency semi-circle centered at 125-200 Hz followed by a straight line with a phase angle of 45° corresponding to the Warburg region (when $\omega >> 2D_{Na}/L^2$, L being the maximum length of the diffusion pathway) related to semi-infinite diffusion (see enlarged view in **Fig. 6b**). Then, for the lowest frequencies, the impedance spectra show quasi-vertical lines corresponding to the finite diffusion process ($\omega << 2D_{Na}/L^2$). This behavior is consistent with that expected for a standard insertion compound [39]. The systematic existence of a Warburg region allows the calculation of the apparent Na chemical diffusion coefficient D_{Na} according to equation (1) [39]:

$$A_w = V_M.(dE/dx)_x / F\sqrt{2}\, S\, D_{Na}^{1/2} \qquad \omega >> 2D_{Na}/L^2 \qquad \text{Eq. (1)}$$

A_w is the Warburg prefactor, V_M is the molar volume of the active material (V_M= 61.223 $cm^3.mol^{-1}$), S is the geometric surface area of the electrode (1cm^2), $(dE/dx)_x$ is the slope, at fixed x, of the equilibrium potential composition curve (**Fig. 6c**).

Figure 6d displays the evolution of the apparent chemical diffusion coefficient of sodium ions D_{Na} as a function of x in Na_xKVO ($0 < x \leq 1$). The rate of sodium transport is higher at the beginning of the sodiation process, around $3.6.10^{-8}$ cm^2 s^{-1} for x = 0.1, then it decreases by one order of magnitude for x = 0.2 ($D_{Na} \approx 3\ 10^{-9}$ cm^2 s^{-1}), and again by one order of magnitude between x = 0.2 and x = 0.5 ($D_{Na} \approx 3\ 10^{-10}$ cm^2 s^{-1} for x = 0.5). In the $0.5 \leq x \leq 0.8$ composition range, D_{Na} remains quite constant then it decreases again to a value of 10^{-10} cm^2 s^{-1} for the most sodiated compositions (x = 0.9 and 1). Hence, the $K_{0.24}V_2O_5$ material obtained after the first cycle promotes Na fast transport in the large interlayer space of 9.32 Å. Then, the D_{Na} evolution is characterized by a moderate decrease limited to ca. one decade during discharge ($0.2 \leq x \leq 1$). This finding is in good correlation with the slight interlayer contraction combined with the increasing Na amount. Scarce data are available on Na^+ mobility in sodiated oxides and bronzes, with very close values

in the range 10^{-12}-10^{-10} cm^2 s^{-1} reported for instance in $Na_{0.33}V_2O_5$ [40, 41], in Na_xCoO_2 [42] and P2-$Na_{0.67}MnO_2$ [43].

3. Conclusion

The present work illustrates the richness of the V_2O_5-based compounds in the search of new promising cathode material for Na-ion batteries. We have successfully prepared the bilayered potassium vanadate $K_{0.5}V_2O_5$ via a reproducible, facile and fast solution technique. The as–synthesized material is characterized by a large interlayer distance of 9.5 Å, i.e. twice that reported for the $Li_{0.5\text{-}1}V_2O_5$ lithium vanadates [44]. A first cycle in the 4 V-1.5 V range at C/10 acts as an activation process, leading to a new KVO composition $K_{0.24}V_2O_5$ due to partial potassium extraction. KVO delivers a high reversible specific capacity of 160 mAh g^{-1} at C/10 with a good capacity retention leading to still 152 mAh g^{-1} after 50 cycles. A detailed XRD and Raman spectroscopy investigation gives evidence for weak structural changes upon discharge and charge: electrochemical sodium insertion-extraction cycles are shown to correspond to weak shrinking-swelling cycles of KVO host lattice whose magnitude is limited to 3% and any significant structural change is detected inside vanadium oxide slabs. The pillaring effect of K^+ ions probably ensures this particular and stable behavior upon cycling. Moreover, the apparent chemical sodium diffusion is not significantly affected during discharge, with values decreasing only by ca. one order of magnitude for $0.2 \leq x \leq 1$ in Na_xKVO. This work sheds light on the concept of pillaring species to stabilize host structures of cathode materials. In that way, such soft breathing of the framework combined with a high cationic diffusivity allows stable cycling properties and good rate capability.

4. Experimental Section

Potassium vanadate $K_{0.5}V_2O_5$ was synthesized by a solution route using 1 g of V_2O_5 (Alfa Aesar 99.995%) and 0.5 g of KVO_3 (Alfa Aesar 99.99%) dissolved in 10 cm^3 of an aqueous solution with 30 cm^3 H_2O_2 (30%). A fast and exothermic reaction takes place leading to a fine precipitate. The solid compound was then heat-treated at 570°C for 5h under argon atmosphere. Elemental analysis by atomic absorption spectroscopy combined with redox titration have been carried out to determine the oxidation state of vanadium ions in the obtained product. This leads to the chemical composition $K_{0.5+/-0.02}V_2O_5$.

XRD experiments were performed using a Panalytical XPert pro apparatus equipped with a X'Celerator detector and using Co Kα radiation (λK_α =1.789 Å). Data are then processed on Eva software to score peaks then CelRef to calculate the lattice parameters. The SEM experiments were carried out using a LEO 1530 instrument. The Raman spectra were obtained with a LaBRAM HR 800 (Jobin-Yvon-Horiba) Raman micro-spectrometer including Edge filters and equipped for signal detection with a back illuminated charge coupled device detector (Spex CCD) cooled by Peltier effect to 200 K. A He:Ne laser (632.8 nm) was used as the excitation source. The spectra were measured in back-scattering geometry. The resolution was about 0.5 cm^{-1}. A 100X objective was used to focus the laser light on sample surface to a spot size of 1 mm^2. To avoid local heating of the sample, the power of the laser beam was adjusted to 0.2-0.5 mW with neutral filters of various optical densities.

Electrochemical experiments were conducted in sodium half-cells consisting into 2032 coin-type cells with a Na foil as the negative electrode, an electrolyte of 1 M $NaClO_4$ in propylene carbonate (PC) containing fluoroethylene carbonate (FEC) additive (2% Vol.) and Whatman glass fiber separator. The KVO positive electrode is prepared by mixing 80 wt % of active material with

7.5 wt % of acetylene black, 7.5 wt % of graphite and 5 wt % of PTFE as binder. About 8 mg of this mix is pressed on a stainless steel grid current collector. The CR2032 coin-cell is assembled in argon-filled glovebox where water and oxygen concentrations were kept less than 1 ppm. Galvanostatic experiments were performed at ambient temperature in the voltage range 1.50 V to 4.00 V, using a VMP3 Biologic apparatus. Impedance measurements were carried out in the frequency range 10^5 Hz to 3 10^{-3} Hz, using the same 2032 coin cell filled with 1M $NaClO_4$ in PC. The excitation signal was 10 mV peak to peak. The positive electrode was made of the same composite electrode as the one used in coin cells. The geometric surface area of the working electrode for impedance measurements is 1 cm^2. The working electrode composition was adjusted by coulometric titration using a low current density corresponding to a C/10 rate. Equilibrium was considered to have been reached when the open circuit voltage remained stable (< 0.2 mV for 1h). The OCV curve has been obtained by performing GITT measurements on the second discharge cycle, using a very low current (C/40 rate) and composition steps of $\Delta x = 0,1$, i. e. current pulses of 100 μA for 30 min followed by a relaxation period for 5 h.

In order to investigate the sodium-driven structural changes in KVO, the cells were discharged to the required composition by galvanostatic reduction at C/10 rate. Equilibrium was considered to be reached when the drift in open-circuit voltage remained less than 0.2 mV h^{-1}. After reaching equilibrium, the cell was opened in the glovebox and the positive electrode was removed, rinsed with dimethyl carbonate (DMC) and placed in specifically designated airtight sample holders to be further analyzed by *ex-situ* X-ray diffraction and Raman spectroscopy. To check the homogeneity, Raman spectra were recorded on 10 different spots of each sample.

Acknowledgments

The authors acknowledge the Agence Universitaire de la Francophonie (AUF), the Vietnam National University, Ho Chi Minh City (projects N° B2011-08-01TĐ and HS2013-76-01, the Ministry of Education and Science of Kazakhstan (grant number AP05136016-ZRABS) and Campus France for their financial support.

Keywords: $K_{0.5}V_2O_5$, layered potassium vanadate, bilayer, cathode material, Na-ion battery

References

[1] D. Larcher, J. M. Tarascon, *Nat. Chem.* **2015**, *7*, 19.

[2] C. Grosjean, P. H. Miranda, M. Perrin, M. and P. Poggi, *Renew. Sust. Energ. Rev*. **2012**, *16* 1735.

[3] S. Komaba, W. Murata, T. Ishikawa, N. Yabuuchi, T. Ozeki, T. Nakayama, A. Ogata, K. Gotoh, K. Fujiwara, *Adv. Funct.Mater.* **2011**, *21*, 3859.

[4] B. L. Ellis, L. F. Nazar, *Curr. Opinion Solid State Mater. Sci.* **2012**, *16*, 168.

[5] V. Palomares, P. Serras, V. Villaluenga, K. B. Hueso, J. Carretero-González, T. Rojo, *Energy Environ. Sci.* **2012**, *5*, 5884.

[6] S. W. Kim, D. H. Seo, X. Ma, G. Ceder, V. Kang, *Adv. Energy Mater*. **2012**, *2*, 710.

[7] V. Palomares, M. Casas-Cabanas, E. Castillo-Martinez, M.H. Han, T. Rojo, *Energy Environ. Sci*. **2013**, *6*, 2312.

[8] H. Pan, Y. S. Hu, L. Chen, *Energy Environ. Sci*. **2013**, *6*, 2338.

[9] M. D. Slater, D. Kim, V. Lee, C. S. Johnson, *Adv. Funct. Mater*. **2013**, *23*, 947.

[10] A. Ponrouch, A. R. Goni, M. R. Palacin, *Electrochem. Comm.* **2013**, *27*, 85.

[11] N. Yabuuchi, K. Kubota, M. Dahbi, S. Komaba, *Chem. Rev*. **2014**, *114*, 11636.

[12] K. Kubota, S. Komaba, *J. Electrochem. Soc*. **2015**, *162*, A2538.

[13] D. Kundu, E. Talaie, V. Duffort, L. F. Nazar, *Angew. Chem. Int. Ed. Engl*., **2015**, *54*, 3431.

[14] J. Y. Hwang, S. T. Myung, Y. K. Sun, *Chem. Soc. Rev*. **2017**, *46*, 3529.

[15] H. Kim, H. Kim, Z. Ding, M. H. Lee, K. Lim, G. Yoon, K. Kang, *Adv. Energy Mater*. **2016**, *6*, 1600943.

[16] Z. Dai, U. Mani, H. T. Tan, Q. Yan, *Small Methods* **2017**, *1*, 1700098.

[17] X. Xiang, K. Zhang, J. Chen, *Adv. Mater.* **2015**, *27*, 5343.

[18] C. Fang, Y. Huang, W. Zhang, J. Han, Z. Deng, Y. Cao, H. Yang, *Adv. Energy Mater.* **2016**, *6*, 1501727.

[19] Y. You, A. Manthiram, *Adv. Energy Mater.* **2018**, *8*, 1701785.

[20] K. West, B. Zachau-Christiansen, T. Jacobsen, S. Skaarup, *Solid State Ion*. **1988**, *28-30*, 1128.

[21] M. Safrany Renard, N. Emery, R. Baddour-Hadjean, J. P. Pereira-Ramos, *Electrochim. Acta* **2017**, *252C*, 4.

[22] R. Baddour-Hadjean, M. Safrany Renard, N. Emery, L. T. N. Huynh, M. L. P. Le, J. P. Pereira-Ramos, *Electrochim. Acta* **2018**, *270*, 129.

[23] S. Tepavcevic, H. Xiong, V.R. Stamenkovic, X. Zuo, M. Balasubramanian,V.B. Prakapenka, C.S. Johnson, T. Rajh, *ACS Nano* **2012**, *6*, 530.

[24] D. Su, G. Wang, *ACS Nano* **2013**, *7*, 11218.

[25] S. Bach, N. Baffier, J. P. Pereira-Ramos, R. Messina, *Solid State Ionics* **1989**, *37*, 41.

[26] J.P. Pereira-Ramos, R. Messina, S. Bach, N. Baffier**,** *Solid State Ion.* **1990**, *40-41*, 970.

[27] H. M. Liu, H. S. Zhou, L. P. Chen, Z. F. Tang, W. S. Yang, *J. Power Sources* **2011**, *196*, 814.

[28] D. Hamani, M. Ati, J.-M. Tarascon, P. Rozier, *Electrochem. Commun*. **2011**, *13*, 938.

[29] M. Guignard, C. Didier, J. Darriet, P. Bordet, E. Elkaim, C. Delmas, *Nat. Mater.* **2013**, *12*, 74.

[30] G. Venkatesh, V. Pralong, O. I. Lebedev, V. Caignaert, P. Bazin, B. Raveau, *Electrochem. Comm.* **2014**, *40*, 100.

[31] H. He, G. Jin, H. Wang, X. Huang, Z. Chen, D. Sun, Y. Tang, *J. Mater. Chem. A*, **2014**, *2*, 3563.

[32] N. Emery, R. Baddour-Hadjean, D. Batyrbekuly, B. Laïk, Z. Bakenov, J. P. Pereira-Ramos, *Chem. Mater.* **2018**, *30*, 5305.

[33] S. Bach, A. Boudaoud, N. Emery, R. Baddour-Hadjean, J. P. Pereira-Ramos, *Electrochim. Acta* **2014**, *119*, 38.

[34] R. Baddour-Hadjean, A. Boudaoud, S. Bach, N. Emery, J. P. Pereira-Ramos, *Inorg. Chem.* **2014**, *53*, 1764.

[35] K. J. Rao, P. A. Ramankrishnan, R. Gadagkar, *J. Solid State Chem*. **1999**, *148*, 100.

[36] Y. Oka, T. Yao, N. Yamamoto, *J. Mater. Chem.* **1995**, *5*, 1423.

[37] R. Baddour-Hadjean, J. P. Pereira-Ramos, C. Navone, M. Smirnov, *Chem. Mater.* **2008**, *20*, 1916.

[38] M. B. Smirnov, E. M. Roginskii, K. S. Smirnov, R. Baddour-Hadjean, J. P. Pereira-Ramos, *Inorg. Chem*. **2018**, *57*, 9190.

[39] C. Ho, I. D. Raistrick, R.A. Huggins, *J. Electrochem. Soc*., **1980**, *127*, 343.

[40] S. Bach, N. Baffier, J. P. Pereira-Ramos, R. Messina, *Solid State Ion*. **1989**, *37*, 41.

[41] D. Jiang, H. Wang, G. Li, G. Li, X. Lan, M. H. Abib, Z. Zhang, Y. Jiang, J. *Electrochem. Soc*., **2015**, *162*, A697.

[42] B. V. R. Reddy, R. Ravikumar, C. Nithya, S. Gopukumar, *J. Mater. Chem.* **2015**, *3*, 18059.

[43] D. Tie, G. Gao, F. Xia, R. Yue, Q. Wang, R. Qi, B. Wang, Y. Zhao, *ACS Appl. Mater. Interf.* **2019**, *11*, 6978.

[44] R. Baddour-Hadjean, E. Raekelboom, J. P. Pereira-Ramos, *Chem. Mater*. **2006**, *18*, 3548.

Figure Captions

Figure 1. SEM images of KVO.

Figure 2. Structural characterizations of KVO (a) X-ray diffraction pattern. Inset: Crystal structure; (b) Raman spectrum. Inset: Schematic V-O polyhedra structure of the double layers.

Figure 3. Electrochemical characterizations and performance of the KVO electrode as cathode material for SIBs. (a) First discharge-charge cycle (C/10 rate); (b) Extended galvanostatic discharge-charge cycles from the second cycle (C/10 rate); c) Discharge capacity as a function of the number of cycles (C/10 rate); (c) Rate capability study in the C/10-5C range.

Figure 4. (a) Evolution of the *001* reflection of KVO electrodes: pristine electrode, electrode after one cycle, electrode during second discharge (x = 0.2, 0.6 and 1 in Na_xKVO), electrode after 2 and 50 cycles at C/10. (b) XRD patterns of initial and cycled KVO electrodes (after 1, 2 and 50 cycles at C/10).

Figure 5. Raman spectra of KVO electrodes: pristine electrode, electrode after one cycle, electrode during second discharge (x = 0.2, 0.6 and 1 in Na_xKVO), electrode after 2 and 50 cycles at C/10.

Figure 6. (a) AC impedance diagrams for Na_xKVO electrodes. (b) Enlarged view of the high frequency region for x = 0.4 (c) Equilibrium (open circuit)-potential versus composition for Na-ion intercalation in KVO obtained from GITT measurements. (d) Evolution of the apparent sodium coefficient D_{Na} and *c* parameter as a function of x in Na_xKVO (second discharge).

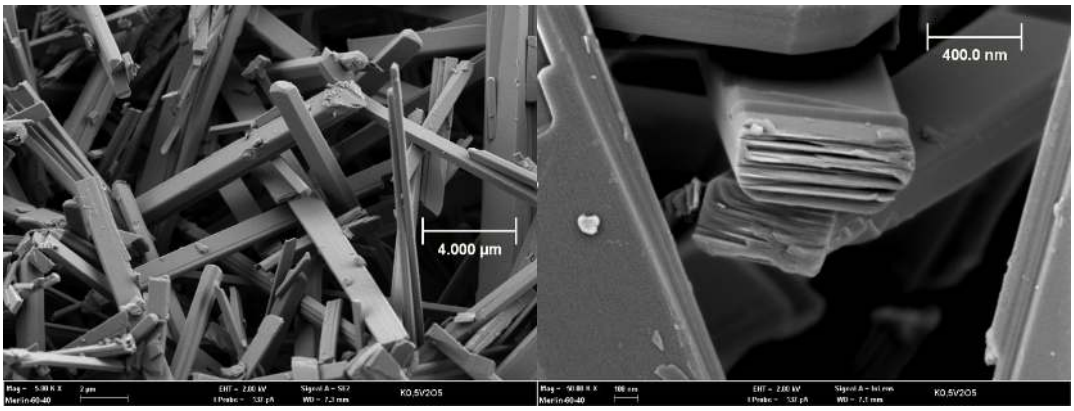

Figure 1. SEM images of KVO

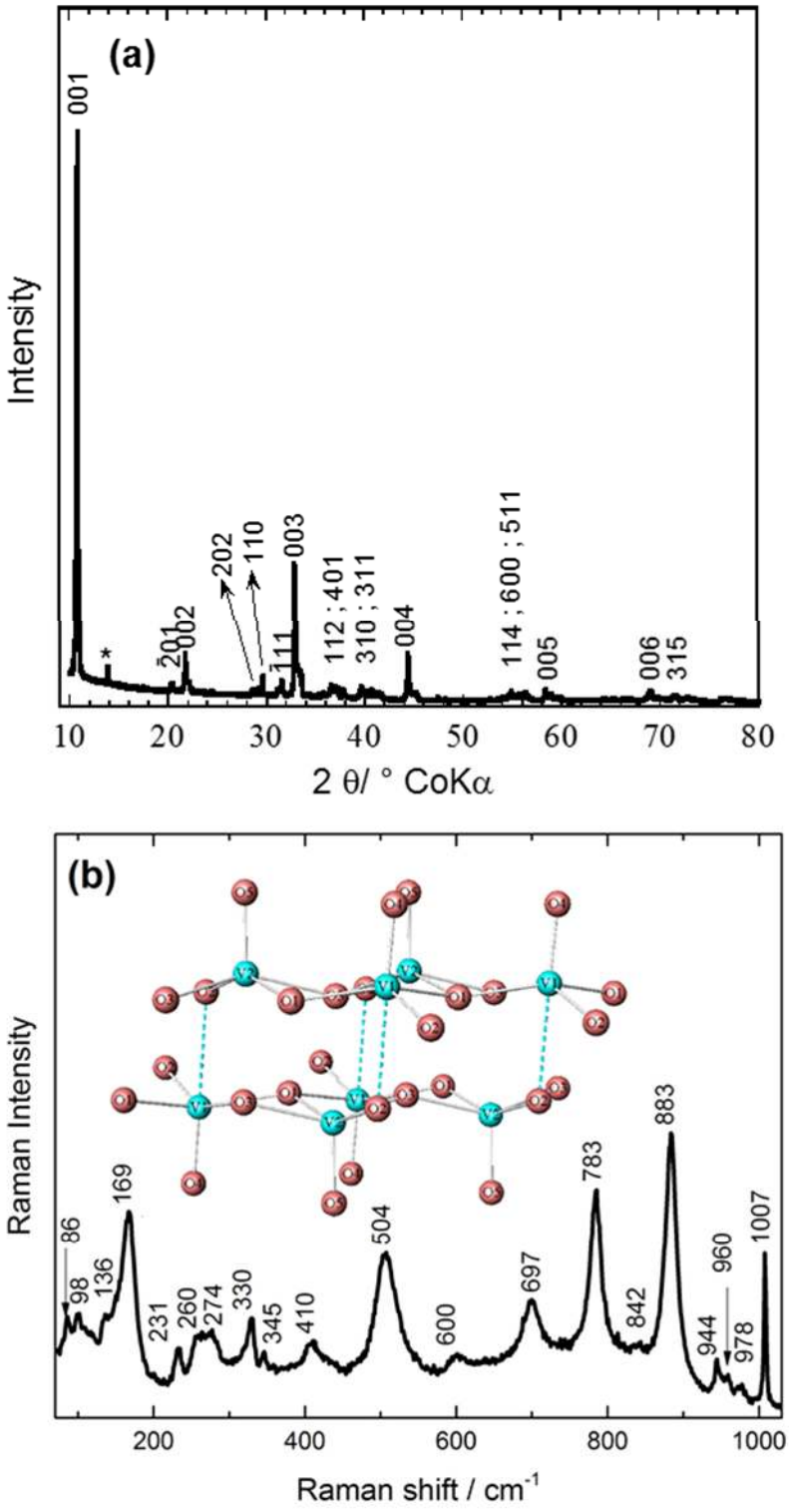

Figure 2. Structural characterizations of KVO (a) X-ray diffraction pattern. *: $K_{0.25}V_2O_5$ impurity Inset: Crystal structure; (b) Raman spectrum. Inset: Schematic V-O polyhedra structure of the double layers.

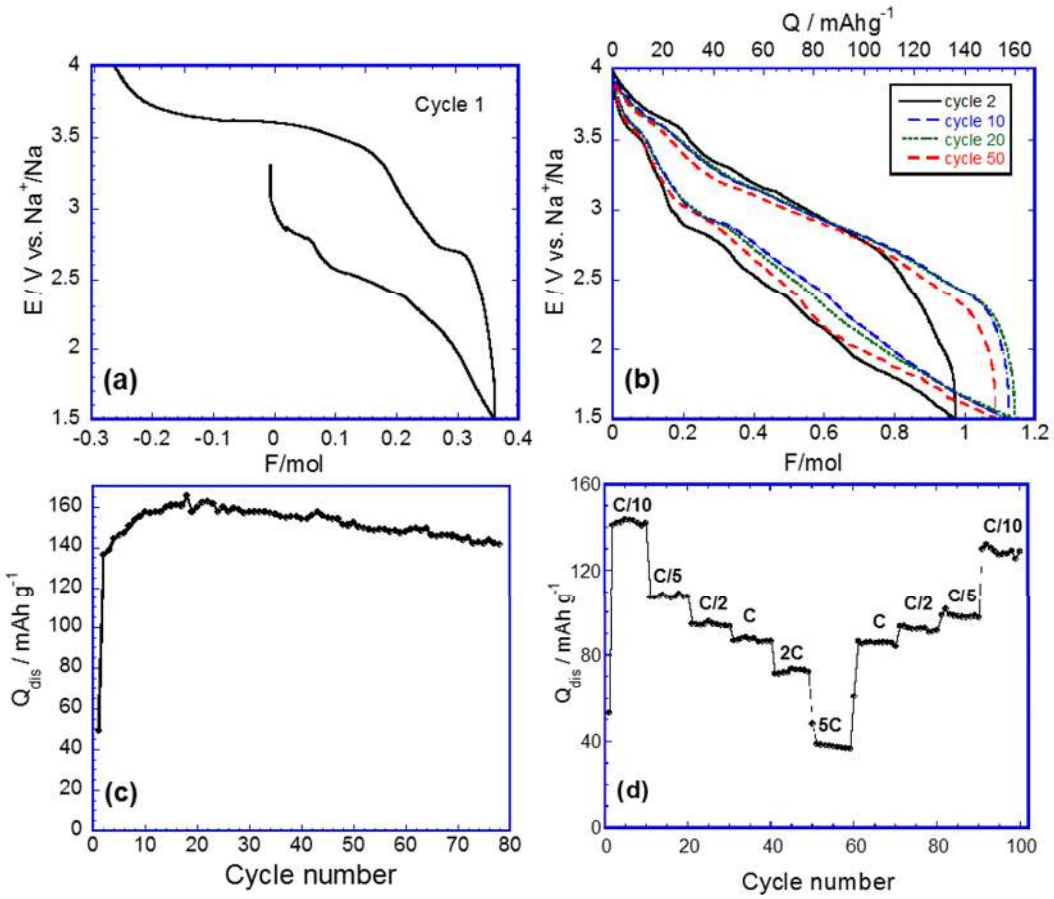

Figure 3. Electrochemical characterizations and performance of the KVO electrode as cathode material for SIBs. (a) First discharge-charge cycle (C/10 rate); (b) Extended galvanostatic discharge-charge cycles from the second cycle (C/10 rate); c) Discharge capacity as a function of the number of cycles (C/10 rate); (d) Rate capability study in the C/10-5C range.

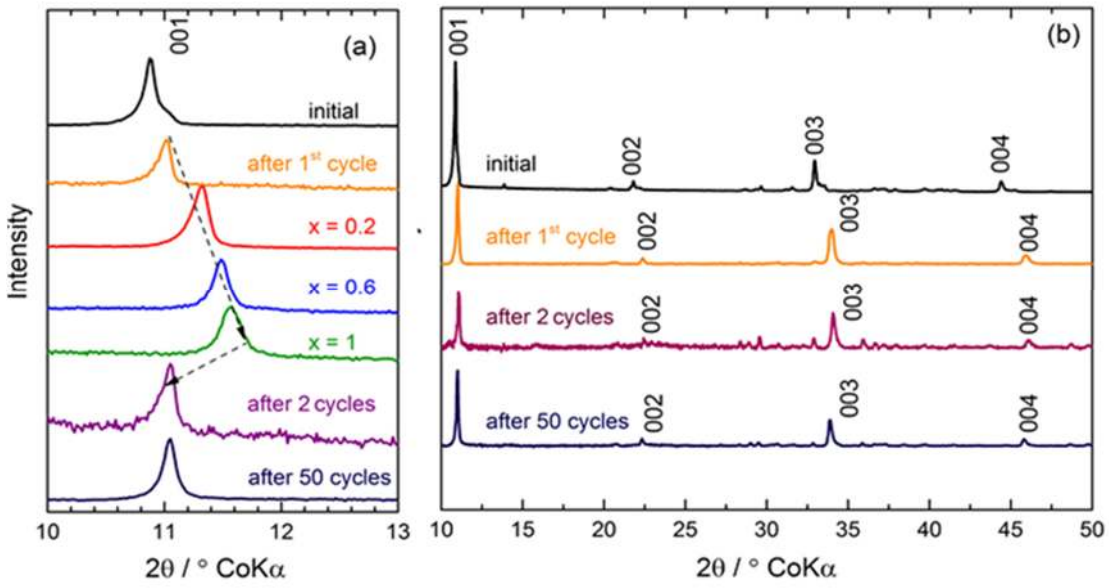

Figure 4. (a) Evolution of the *001* reflection of KVO electrodes: pristine electrode, electrode after one cycle, electrode during second discharge (x = 0.2, 0.6 and 1 in Na_xKVO), electrode after 2 and 50 cycles at C/10. (b) XRD patterns of initial and cycled KVO electrodes (after 1, 2 and 50 cycles at C/10).

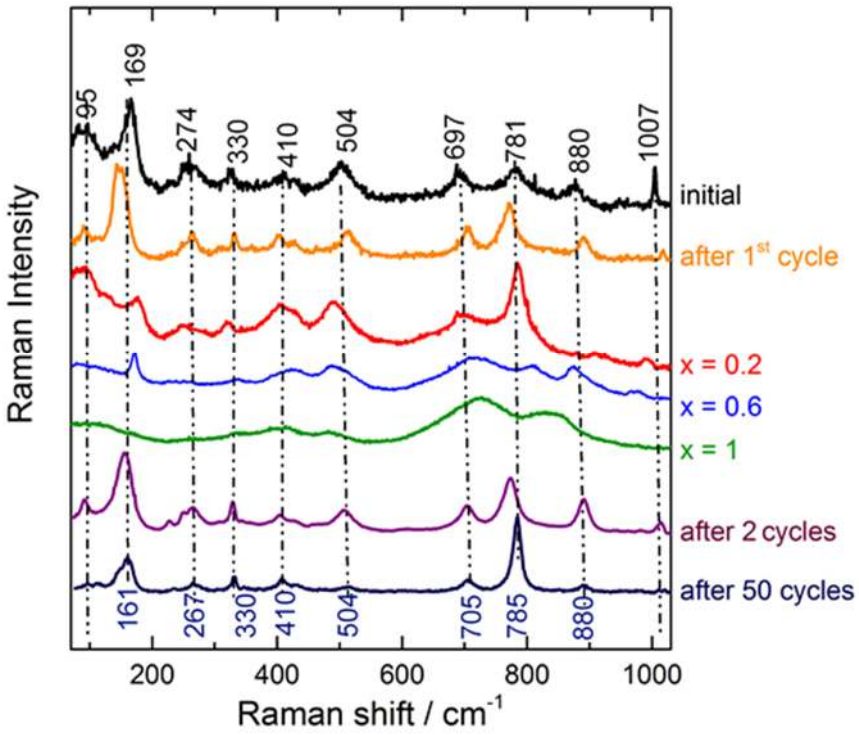

Figure 5. Raman spectra of KVO electrodes: pristine electrode, electrode after one cycle, electrode during second discharge (x = 0.2, 0.6 and 1 in Na_xKVO), electrode after 2 and 50 cycles at C/10.

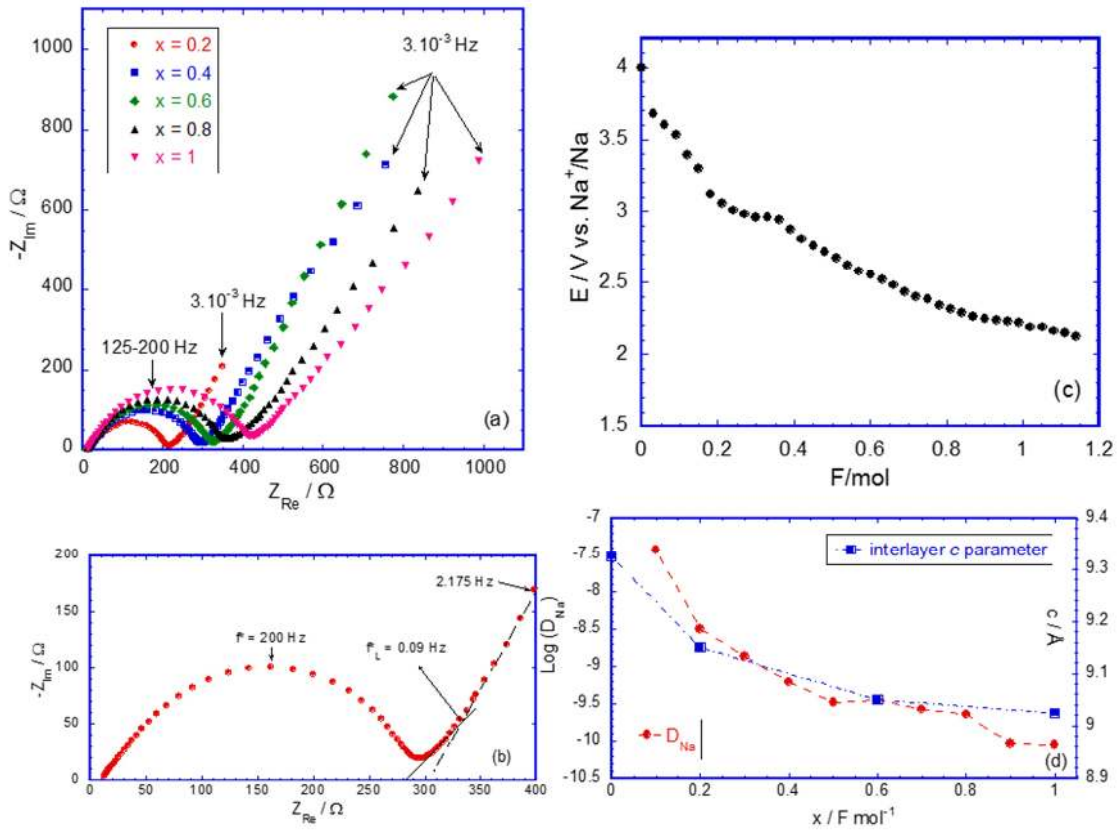

Figure 6. (a) AC impedance diagrams for Na_xKVO electrodes. (b) Enlarged view of the high frequency region for x = 0.4 (c) Equilibrium (open circuit)-potential versus composition for Na-ion intercalation in KVO obtained from GITT measurements. (d) Evolution of the apparent sodium coefficient D_{Na} and *c* parameter as a function of x in Na_xKVO (second discharge).